Cell Reports

Report

State-Dependent Changes in Perception and Coding in the Mouse Somatosensory Cortex

Graphical Abstract

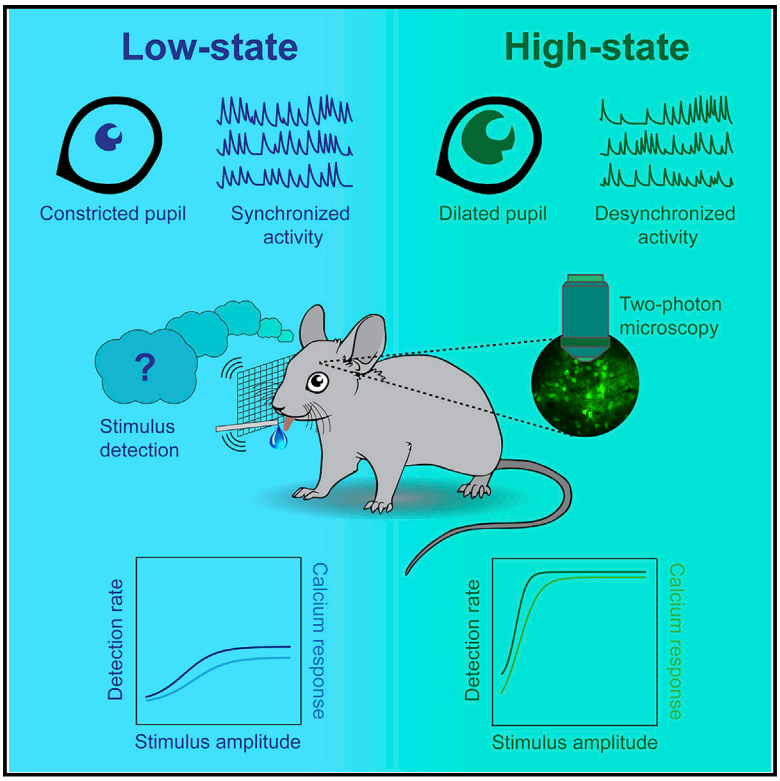

Highlights

- Behavioral state and calcium signal in somatosensory cortex predict choice outcome
- Neurometric curves mirrors psychometric performances for each behavioral state
- Network synchrony and pupil diameter are coupled to changes in behavioral state
- High behavioral state results in enhanced information transmission

Authors

Conrad C.Y. Lee, Ehsan Kheradpezhouh, Mathew E. Diamond, Ehsan Arabzadeh

Correspondence

conrad.lee@anu.edu.au

In Brief

Lee et al. investigate how information processing in the mouse somatosensory cortex varies across behavioral states. High behavioral states defined by enhanced detection and dilated pupils correspond to enhanced sensory-evoked responses and low population variability. These changes in neuronal activity improve information transmission and stimulus encoding at the population level.

Lee et al., 2020, Cell Reports *32*, 108197
September 29, 2020
https://doi.org/10.1016/j.celrep.2020.108197

CellPress

Cell Reports

CellPress
OPEN ACCESS

Report

State-Dependent Changes in Perception and Coding in the Mouse Somatosensory Cortex

Conrad C.Y. Lee,[1,2,4,*] Ehsan Kheradpezhouh,[1,2] Mathew E. Diamond,[2,3] and Ehsan Arabzadeh[1,2]
[1]Eccles Institute of Neuroscience, John Curtin School of Medical Research, The Australian National University, Canberra, ACT 2601, Australia
[2]Australian Research Council Centre of Excellence for Integrative Brain Function, The Australian National University Node, Canberra, ACT 2601, Australia
[3]Cognitive Neuroscience, International School for Advanced Studies (SISSA), Trieste, Italy
[4]Lead Contact
*Correspondence: conrad.lee@anu.edu.au
https://doi.org/10.1016/j.celrep.2020.108197

SUMMARY

An animal's behavioral state is reflected in the dynamics of cortical population activity and its capacity to process sensory information. To better understand the relationship between behavioral states and information processing, mice are trained to detect varying amplitudes of whisker-deflection under two-photon calcium imaging. Layer 2/3 neurons in the vibrissal primary somatosensory cortex are imaged across different behavioral states, defined based on detection performance (low to high-state) and pupil diameter. The neurometric curve in each behavioral state mirrors the corresponding psychometric performance, with calcium signals predictive of the animal's choice. High behavioral states are associated with lower network synchrony, extending over shorter cortical distances. The decrease in correlation across neurons in high state results in enhanced information transmission capacity at the population level. The observed state-dependent changes suggest that the coding regime within the first stage of cortical processing may underlie adaptive routing of relevant information through the sensorimotor system.

INTRODUCTION

The precision with which sensory neurons represent the environment constrains the quality of subsequent processing in higher cortical areas, ultimately influencing the behavior of the organism. However, the activity of cortical neurons can be explained by considering externally generated afferent (sensory) signals in conjunction with internally generated activity in the brain (McGinley et al., 2015). This internally generated activity depends largely on the behavioral state of the animal. The behavioral state can range from active engagement with the environment to quiet wakefulness and sleep. Changes in the behavioral state are reflected in the population activity of cortical neurons (Sabri and Arabzadeh, 2018) and are often manifested in the level of correlated activity—from desynchronized during active engagement to synchronized during sleep (Harris and Thiele, 2011).

The ecological demands of natural environments vary over time, and animals benefit from tuning neuronal processing to match current behavioral goals (Kayser et al., 2005). Here, we investigate how the efficiency of sensory processing and the conversion of sensory information into a decision depend on the behavioral state. To achieve this, we trained mice to detect vibrations applied to their whiskers while monitoring population activity in the vibrissal area of the primary somatosensory cortex (vS1) under two-photon calcium imaging. Rodents are frequently active in darkness and can detect minute vibrations from approaching predators and produce vibration signals to warn their colony (Randall, 2010). We use this highly efficient sensory system to establish how the dynamics of vS1 populations vary from state to state.

RESULTS

Detection Performance and Cortical Activity in Response to Vibration Stimuli

Head-fixed mice (n = 7) were injected with GCaMP6*f* in the vS1 cortex and trained to perform a whisker vibration detection task (Figure 1A). A series of pulsatile vibrations was presented via a piezo-driven mesh on the left whisker pad at amplitudes of 0, 10, 20, 40, or 80 μm. Mice were rewarded for licking the spout on trials with vibration (10, 20, 40, and 80 μm); licking in the absence of vibration (0 μm) was not rewarded (Figure 1B). To capture time-varying global arousal states, mice were allowed to perform this task for an extended period (median session duration, 52 min; 300–400 trials). Mice successfully refrained from licking when the vibration was absent (Figure 1C; lick rate on stimulus absent trials was not different from pre-stimulus lick rate; p = 0.136, Wilcoxon rank-sum). In the presence of the vibration, three measures were found to vary in a graded manner with stimulus amplitude. First, mice licked at a higher rate with increasing amplitude (Figure 1C; ROC analysis, Figure S1A). Second, they showed faster response times with increasing amplitude (Figures 1C and S1B). Third, they showed increased detection rates, with the shape of a compressive

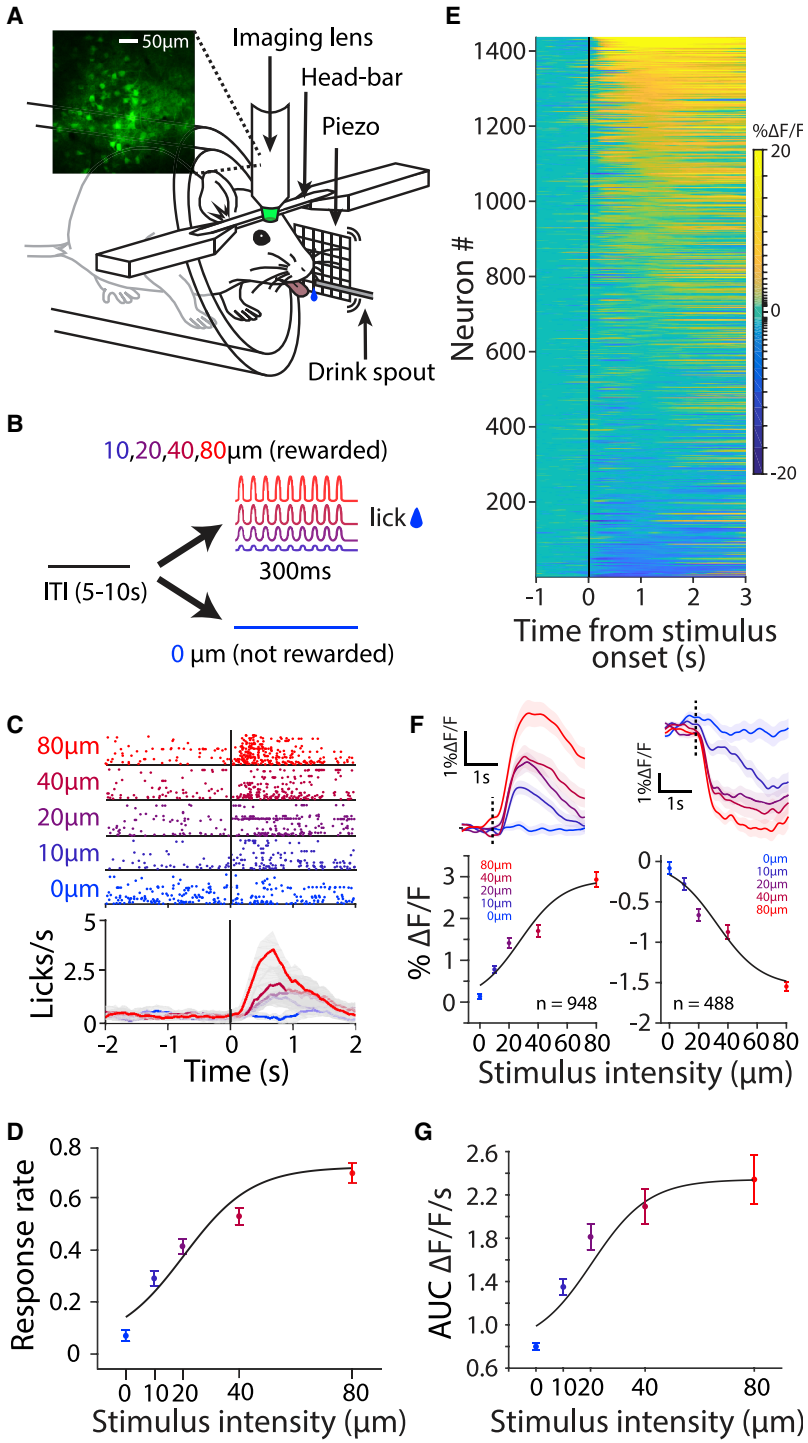

Figure 1. Characterization of Behavior and Calcium Response

(A) As mice performed the vibration detection task, we imaged neuronal activity from the vibrissal area of the primary somatosensory cortex using 2-photon excitation microscopy (GCaMP6*f*) (scale bar indicates 50 μm). Stimuli were presented via a mesh place on the left whisker pad, and sucrose reward was provided via a capacitive sensing spout.

(B) A 300-ms, 40-Hz vibration stimulus was presented at 1 of 5 intensities (0, 10, 20, 40, 80 μm). Licking the spout during stimulus presentation (10–80 μm) resulted in sucrose reward. Licking the spout at any other time did not result in delivery of sucrose. Each stimulus presentation had an intertrial/stimulus interval of 5–10 s.

(C) Licking profile of an example session. In the raster plot, each lick is represented as a dot and each row represents a trial. Each color represents a different intensity. Average peri-stimulus time histograms are presented with the same color notation. The shaded error bars represent SEMs.

(D) Hit rate for all mice (n = 7) as a function of stimulus intensity. The line represents the best fit of a cumulative Gaussian function. The error bars represent SEMs.

(E) Every row represents 1 cell (n = 1,436). All trials of the 80-μm vibration are averaged for each cell. The cells are sorted based on their average activity 1-s post-stimulus onset. The scale is logarithmic.

(F) Average calcium trace in response to all stimulus intensities (top), along with corresponding neurometric curve (bottom). Fluorescence values are calculated from 0- to 1-s post-stimulus window. Left panels, positive responding cells of (E) (n = 948). Right panels, negative responding cells of (E) (n = 488). The error bars represent SEMs.

(G) Response modulation as a function of stimulus intensity for all cells. Responses are calculated by average area under the curve (0- to 1-s post-stimulus window). The continuous line represents the best fit of a cumulative Gaussian function. The error bars represent SEMs.

sigmoid (Figure 1D). Overall, the behavioral results indicate that the stimulus intensities covered a range from near-threshold to reliably detectable.

We used 2-photon calcium imaging to monitor layer 2/3 (L2/3) neurons (Figure 1A, inset). Overall, we recorded a total of 1,436 cells across 7 mice (Figure 1E). Calcium fluorescence was modulated by the onset of the vibration with a heterogeneous profile, including stimulus-evoked increases and decreases in activity. Figure 1E illustrates the heterogeneity by sorting cells based on their average 1-s evoked response. Regardless of sign of modulation, across the entire imaged population, neurons showed a graded response to stimulus amplitude: excited neurons (n = 948) became more excited; inhibited neurons (n = 488) became more inhibited (Figure 1F). Restricting analysis to significantly responsive cells also showed the same profile (Figure S1C: excited neurons, n = 343; Figure S1D: inhibited neurons, n = 274). To combine both excited and inhibited neurons, we computed the area under the 1-s fluorescence trace for all imaged neurons as a measure of stimulus-evoked modulation (Figure 1G). Area under the curve values exhibited a graded response to the stimulus in the form of a sigmoidal function (Figure 1G), which closely matched the relation of response rate to stimulus intensity (Figure 1D) (behavioral response

CellPress
OPEN ACCESS

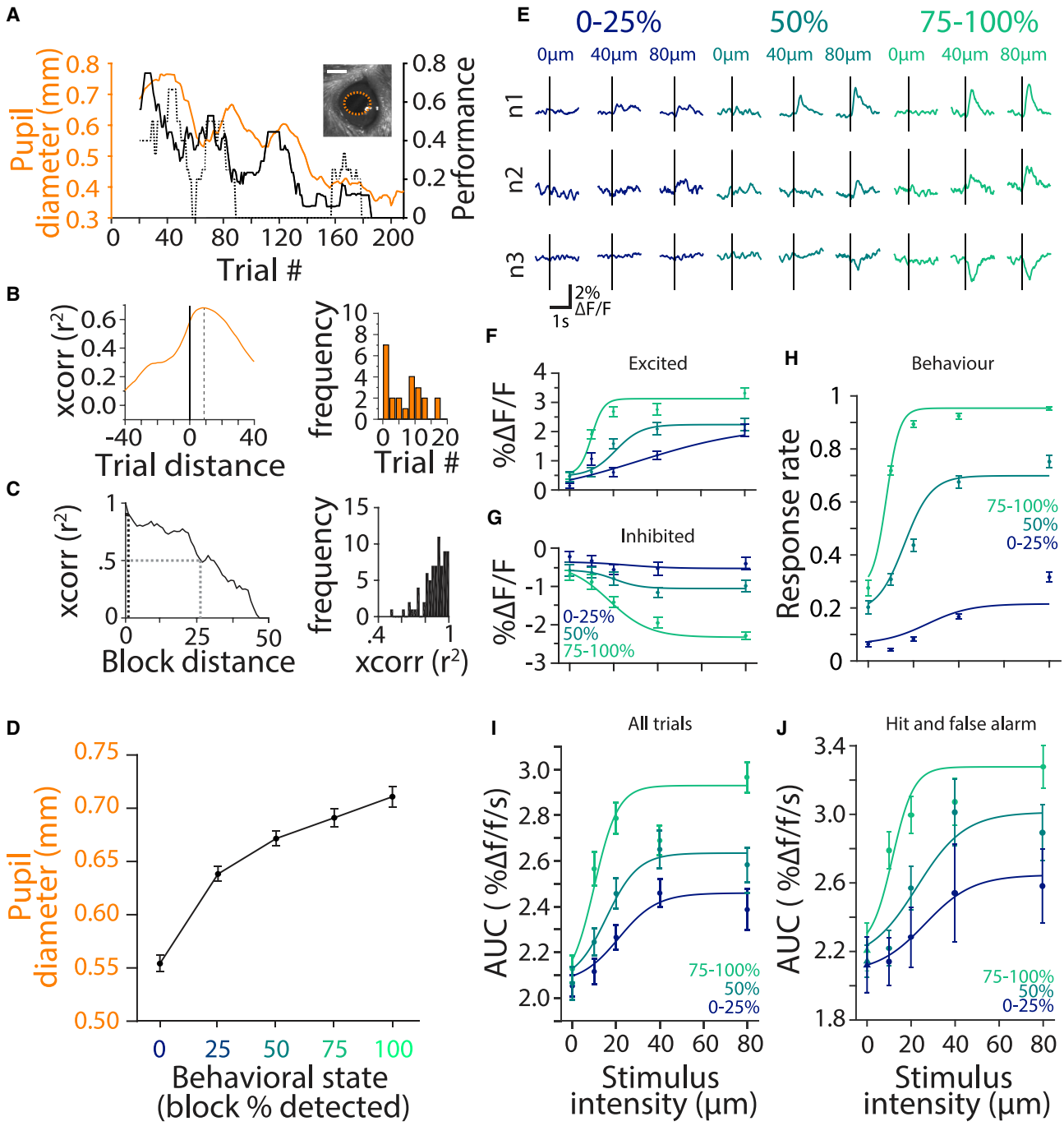

Figure 2. Behavioral State Modulates Psychometric and Neurometric Response Profile

(A) Changes in pupil diameter (orange), detection performance (black), and false alarm rate (black dashed line) of an example session. Lines indicate 10 trial sliding averages of respective measurements. Inset, screenshot of example pupil and estimation of pupil size. The scale bar indicates 0.5 mm.

(B) Left, cross-correlogram of performance and pupil diameter in an example session. Right, trial location of peak correlation across all of the sessions.

(C) Left, auto-correlation of performance in an example session. The black dashed line represents the correlation coefficient at 1 block distance (5 trials). The gray dashed line represents the block distance at 0.5 correlation coefficient. Right, frequency distribution of correlation coefficient at 1 block distance across all of the sessions.

(D) Pupil diameter (average pupil size −5 to 0 s from stimulus onset) as a function of behavioral state. The error bars represent SEMs.

(E) Average response of 3 example cells to 0, 40, and 80 μm at 0%–25% (blue), 50% (turquoise), and 75%–100% (green) behavioral states.

(F) Neurometric response of top 50% responding cells for 3 behavioral states. The error bars represent SEMs.

(G) Neurometric response of bottom 50% responding cells for 3 behavioral states. The error bars represent SEMs.

(legend continued on next page)

function inflection point 11.3 μm; fluorescence response function inflection point 12.1 μm), suggesting fluorescence magnitude as a neurometric correlate of the psychometric detection function.

Behavioral State Affects Single-Cell Coding of Stimulus Intensity

As mice were allowed to perform the detection task for an extended period each session, we were able to image the same cells over different levels of arousal. Behavioral performance was not static—it waxed and waned throughout each session between periods of high and low detection rates (Figure 2A, black). The observed fluctuations in detection rate across time were correlated with pupil diameter (Figure 2A, orange; Video S1). Cross-correlation analysis revealed a moderate coupling between pupil dilation and detection performance (Figure 2B, right). The temporal relationship was consistently observed across sessions, with pupil diameter lagging behind performance by a median of 9.2 trials (Figure 2B, left). On selected sessions, we observed a general slowly progressing decrease in performance. This may reflect changes in the animal's motivation over time. We examined this by taking into account the false alarm rate (response to stimulus absent trials) across time (Figure 2A, dashed black line). On average, we observed a small but significant correlation between hit rate and false alarm rate over time ($r = 0.22$, $p = 5.4 \times 10^{-9}$ **). This slow time course of motivation could have a different impact on sensory coding than the faster trial-by-trial variability. Overall, across all of the recorded sessions, mice predominately correctly rejected stimulus-absent trials.

Next, we quantified the temporal profile of changes in behavioral performance. Stimuli were distributed into blocks of 5 trials, within which 4 vibration amplitudes (10, 20, 40, and 80 μm) were presented in a randomized fashion along with the no-vibration trial (0 μm amplitude). This allowed us to quantify the behavioral state by calculating the detection rate within each block (0%: no detection; 100%: all 4 amplitudes detected). (Hereafter, we refer to this block detection rate as "behavioral state.") To capture the temporal dynamics of state changes, we computed the autocorrelation of behavioral state for each session (Figure 2C, left). Across all of the sessions, the analysis revealed a high correlation ($r = 0.82$) between adjacent blocks (5 trials) and an average half-width of 27 blocks. Overall, the behavioral state showed a robust correlation with pupil diameter; as the detection rate increased, pupil diameter increased (Figure 2D) and dilation variance decreased (Figure S2A). Similarly, hit rate increased as pupil diameter increased (Figure S2B).

Neuronal activity in vS1 varied with behavioral state. Three example cells (Figure 2E) show typical modulations of evoked response with state. As state transitioned from low (0%–25%) to high (75%–100%), response magnitude for a given stimulus amplitude increased—excited cells became more excited and inhibited cells became more inhibited (Figure S2C). How do these response modulations influence the coding efficiency in vS1 cortex? Figures 2F and 2G plot the calcium response functions separately for excited and inhibited cells. Consistent with the response profile of the example cells, neurometric functions both for the excited and inhibited populations became steeper as the state transitioned from low to high, in a manner suggestive of gain modulation. The same profile was found when restricted to significantly responsive cells (Figures S2D and S2E) or when sorting cells based on a smaller, 50-ms window (Figure S2F). Next, we obtained behavioral psychometric curves (Figure 2H) and compared them with the population neurometric function across all 1,436 cells by calculating the area under the curve values as before (Figure 2I). The calcium response profiles showed a leftward shift as the state transitioned from low to high (inflection points for 0%–25%, 50%, and 75%–100% at 22, 15, and 8 μm, respectively). The leftward shift was accompanied by a gain modulation of population neurometric functions; the magnitude of change in fluorescence (%ΔF/F) at the inflection point increased as the state transitioned from low to high (for 0%–25%, 50%, 75%–100% at 2.28, 2.35, and 2.40%ΔF/F, respectively). Again, there was a remarkable correlation between the neurometric and psychometric functions across states (Figure 2H; inflection points for 0%–25%: 26 μm; 50%: 16 μm; 75%–100%: 8 μm). The observation of the elevated neuronal response profile during the high state may have resulted from the higher proportion of hit trials. Previous studies have shown the response of vS1 to be modulated by choice (Poulet and Crochet, 2019; Yamashita and Petersen, 2016; Yang et al., 2016). We performed two additional analyses to better dissociate the sensory component of the evoked response from the motor/decision component. When restricting our analysis to only hit trials, we observed a similar response profile (Figure 2J). In the same light, when restricting our analysis to the first 50 ms (to isolate biphasic motor response observed in experiments using electrophysiology; Sachidhanandam et al., 2013; Yamashita and Petersen, 2016), we also observed a similar response profile (Figure S2G). Finally, given the changes in overall motivation observed by the decreasing false alarm over time (Figure 2A, dashed line), we isolated blocks of trials in which false alarm rates were zero (see Method Details). This analysis also produced similar results (Figure S2H). Overall, as the state transitioned from low to high, the calcium response profile became steeper, indicating a positive gain modulation.

Behavioral State Affects Population Coding of Stimulus Intensity

How does behavioral state affect the dynamic interaction between cells and in turn determine the efficiency of the population

(H) Psychometric curves averaged across all mice for 3 behavioral states (blue: 0%–25%; turquoise: 50%; green: 75%–100%). The continuous line represents the best fit of a cumulative Gaussian function to each of the 3 behavioral states. The error bars represent SEMs.

(I) Neurometric response of all cells as calculated by area under the curve (0- to 1-s window post-stimulus onset) for 3 behavioral states. The continuous line represents the best fit of a cumulative Gaussian function to each of the 3 behavioral states. The error bars represent SEMs.

(J) Neurometric response of all cells as calculated by area under the curve (0- to 1-s window post-stimulus onset) of trials in which animal responded (hit for stimulus present, filled circle; false alarm for stimulus absent, filled triangle) in 3 behavioral states. The continuous line represents the best fit of a cumulative Gaussian function to each of the 3 behavioral states. The error bars represent SEMs.

CellPress
OPEN ACCESS

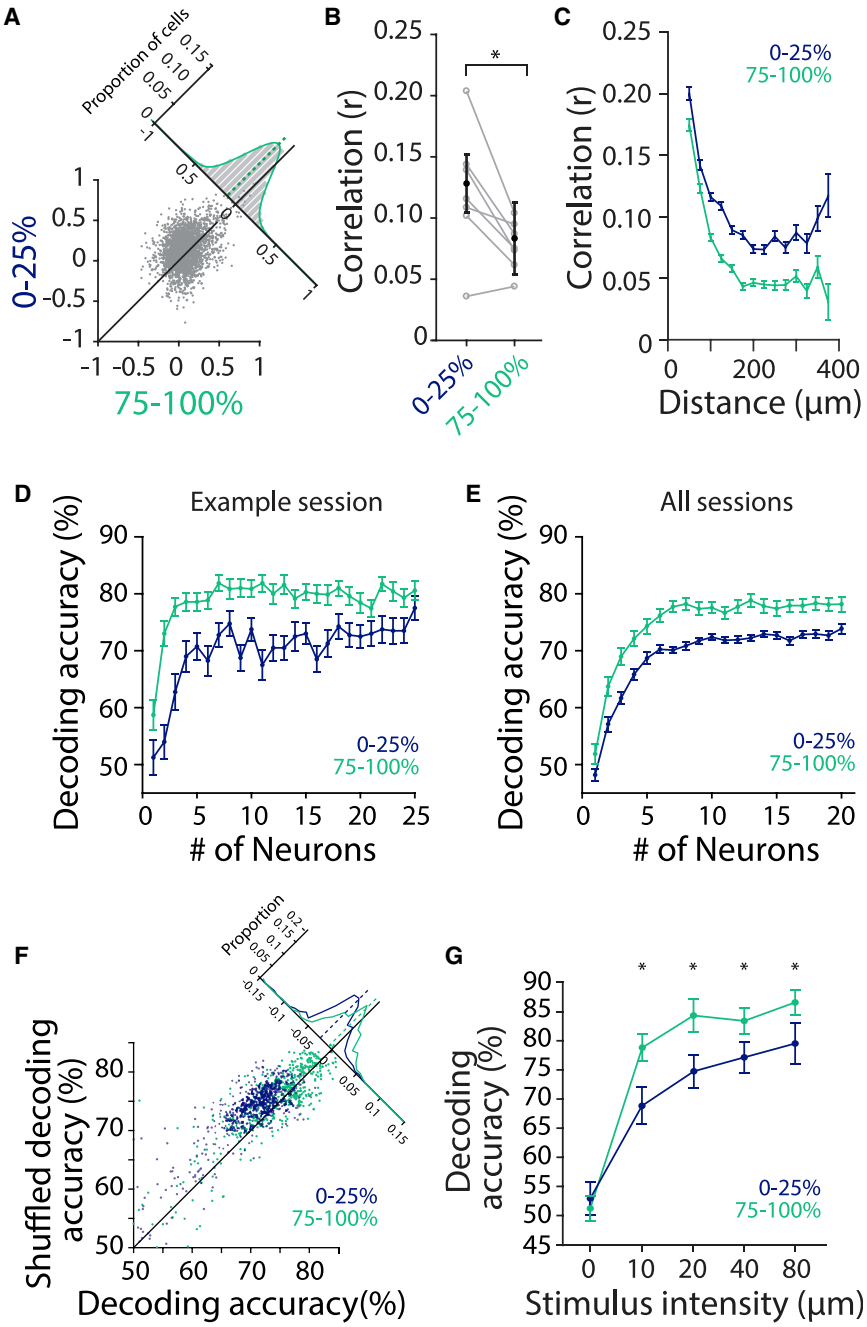

Figure 3. Noise Correlation and Decoding Accuracy across Behavioral States

(A) Noise correlation of cells in example session between 0%–25% (blue) and 75%–100% (green). Cells in the 0%–25% blocks exhibit higher noise correlation than the 75%–100%. The inset indicates histogram distribution from the line of equivalence.

(B) Noise correlation for each mouse between 0%–25% and 75%–100% (gray). Average noise correlation averaged across all mice between 0%–25% and 75%–100% (black). The error bars represent SD.

(C) Noise correlation averaged across all mice as a function of cell distance. Blue: 0%–25%; green: 75%–100%. The error bars represent SEMs.

(D) Linear decoding accuracy of an example session for 20 μm between 0%–25% (blue) and 75%–100% (green) as a function of the number of cells. The error bars represent SEMs.

(E) Linear decoding accuracy across all sessions for 20 μm between 0%–25% (blue) and 75%–100% (green) as a function of the number of cells, up to the median population size (20 cells). The error bars represent SEMs.

(F) Comparison of linear decoding accuracy of 20-μm stimulus between decorrelated trials (by shuffling) and actual data. Each dot denotes the average accuracy of a particular session of a particular population size.

(G) Average linear decoding accuracy for each session across stimulus intensities using all significantly responsive cells recorded simultaneously. *$p < 0.01$, Wilcoxon rank-sum test. The error bars represent SEMs.

code? It is well known that stimulus-independent trial-to-trial correlation in activity (noise correlation) limits the quantity of information that any neuronal population can carry about the sensory input (Averbeck et al., 2006; Kohn et al., 2016; Pola et al., 2003). We therefore quantified how noise correlation varied across behavioral states. The analyses revealed a significant decrease in pairwise correlation ($p = 2.75 \times 10^{-48}$**, Student's t test) as the state transitioned from low to high (Figure 3A). This trend was consistent across mice (Figure 3B, $p = 0.012$*, Student's t test). Whisker tracking indicated no significant difference in whisker movement between behavioral states (Figure S3; Video S2). Noise correlation varied with distance; nearby cells exhibited higher noise correlation compared to distant pairs (Figure 3C). From 25 to 400 μm, the dropoff in correlation with distance was steeper and to a lower plateau in the higher behavioral state.

Theoretically, noise correlation is expected to reduce the efficiency of information transmission (Averbeck et al., 2006; Safaai et al., 2013). We performed linear discriminant analysis to quantify how reliably an ideal observer of the population activity could decode stimulus intensity. Given the levels of noise correlation (Figures 3A–3C), we expected greater information transmission efficiency at higher states. This hypothesis was confirmed by characterizing the accuracy of decoding the presence (versus absence) of the 20-μm vibration with growing population size (Figure 3D, example session; Figure 3E, average across all of the sessions). For the same population of neurons, decoding accuracy rose more sharply and plateaued at a higher decoding performance in the high state compared to the low state. To examine the contribution of noise correlation to decoding accuracy, we decorrelated the activity of neurons by shuffling trials. As shown in Figure 3F,

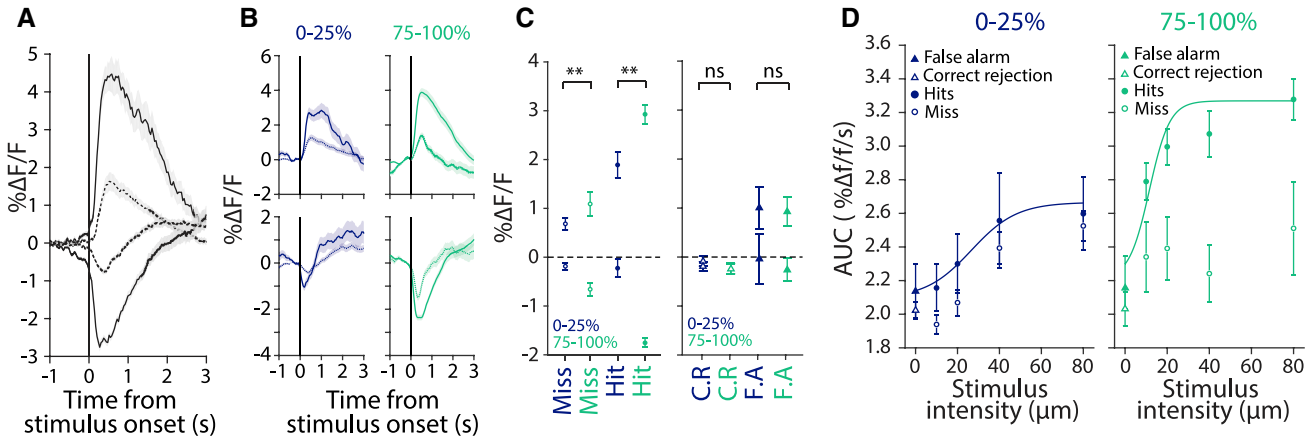

Figure 4. Choice-Correlated Activity in High and Low State

(A) Average traces of top 25% and bottom 25% responding cells in response to hit (solid line) and miss (dash line) trials. The shaded error area represents SEMs.

(B) Average traces of top 25% and bottom 25% responding cells to hit and miss trials in low behavioral state (0%–25%, blue) and high behavioral state (75%–100%, green). The shaded error area represents SEMs.

(C) Left: 1 s average response of top 25% and bottom 25% responding cells for hit and miss trial in low behavioral state (0%–25%, blue) and high behavioral state (75%–100%, green). Right: 1 s average response of top 25% and bottom 25% responding cells for correct rejection and false alarm trial in low behavioral state (0%–25%, blue) and high behavioral state (75%–100%, green). The error bars represent SEMs.

(D) Average calcium response profile of cells as calculated by the area under the curve (0- to 1-s window post-stimulus onset) for hits (filled circles), misses (open circles), false alarms (filled triangle), and correct rejections (open triangle) across 3 behavioral states. The error bars represent SEMs.

decorrelation led to a significant increase in decoding accuracy in both the low state (blue; $p = 4.31 \times 10^{-76}$ **, Wilcoxon sign-rank) and the high state (green; $p = 3.04 \times 10^{-14}$**, Wilcoxon sign-rank). However, the decorrelation-induced increase in accuracy was significantly greater in the low state than in the high state ($p = 4.57 \times 10^{-32}$ **, Wilcoxon rank-sum). Finally, the enhanced population coding in the high state was systematically observed across imaging sessions with various population sizes and was present across all stimulus intensities (Figure 3G).

Calcium Responses Reflect Choice Outcome

We asked how the neuronal responses in vS1 correlate with a mouse's upcoming detection behavior. With data from all of the behavioral states pooled, the average response magnitude on hit trials was significantly larger than on miss trials for both excited and inhibited cells (Figure 4A, 500-ms window post-stimulus, excited: $p = 1.93 \times 10^{-21}$**; inhibited: $p = 3.08 \times 10^{-8}$,** Wilcoxon rank-sum). As revealed in Figures 4B and 4C (ungrouped categories in Figure S4A), there was a greater difference between hit and miss response magnitudes in high states (75%–100% detection blocks) compared to low states (0%–25% detection blocks). We quantified the state-related differences in cortical activity after controlling for trial outcome (hit versus miss). Hit trials during the high state elicited a significantly greater response (both excitation and inhibition) than hit trials during the low state (excitation: $p = 1.33 \times 10^{-10}$**; inhibition: $p = 1.40 \times 10^{-10}$**). Similarly, miss trials during high state elicited a significantly greater response than miss trials during low state (excitation: $p = 2.6 \times 10^{-6}$; inhibition: $p = 2.9 \times 10^{-10}$**). Given that detection rate and calcium responses were both modulated by the strength of the stimulus (Figures 1D and 1G), the proportion of stimulus intensities contributing to hit and miss trials could be different between high and low states. Nevertheless, a further examination of calcium responses across stimulus intensity for hit and miss trials provided similar state-dependent modulations (Figure 4D); overall, hit trials produced larger calcium response than miss trials across stimulus intensities. A complementary analysis revealed a similar pattern of results when the behavioral state was defined after excluding the current trial outcome (Figure S4B). Finally, we examined the neuronal activity of stimulus-absent trials. For both correct rejection and false alarm trials, there was no significant difference in calcium response between high states (75%–100% detection blocks) and low states (0%–25% detection blocks) (false alarm: $p = 0.66$; correct rejection: $p = 0.62$, Wilcoxon rank-sum; Figure 4C). These findings imply that the changes in behavioral performance may be defined by the quality of stimulus encoding within vS1.

DISCUSSION

We investigated the relationship between behavioral state, sensory-evoked responses in single neurons, and the dynamics of vS1 neuronal population in head-fixed mice performing a vibration detection task. As the mice transitioned from low to high behaving states, neurometric curves shifted toward lower stimulus intensities. This enhanced detection sensitivity at the level of single neurons was accompanied by a state-induced reduction in correlated activity across neurons.

The whisker pathway provides a suitable model to study sensory coding efficiency due to the ecological relevance of whisker touch in rodent behavior. Using its whiskers, a rodent can complete complex behavioral tasks, such as discriminating textures (Diamond et al., 2008; von Heimendahl et al., 2007; Zuo et al., 2015), discriminating vibrations (Adibi et al., 2012; Fassihi

et al., 2014), and localizing objects (Kwon et al., 2016; O'Connor et al., 2010). In the absence of a tactile behavioral task, whisker movement has been used as a proxy for cortical state (Eggermann et al., 2014; Muñoz et al., 2017; Poulet and Petersen, 2008; Poulet et al., 2012), in which a large amplitude of whisker movement is considered an active exploratory state, while no whisker movement is considered as quiet-quiescence. However, when seeking to acquire signals from a moving object (i.e., a vibration), rodents can actively immobilize their whiskers to optimize sensitivity (Diamond and Arabzadeh, 2013; Lee et al., 2016, 2019). Here, we focused on this active yet immobile "receptive mode" to investigate state-induced changes in neuronal activity.

We observed a heterogeneous response to the vibration, with some cells excited and others inhibited. As behavioral state transitioned from low to high, excited cells became more excited and inhibited cells became more inhibited (Figures 2 and S2C). Overall, the high state decreased synchrony (Figures 3A–3C) while enhancing the modulations in response. This finding is consistent with observations in the visual cortex (Speed et al., 2019), but different from previous observations in the vS1 cortex, in which the desynchronized state produced lower evoked responses (Otazu et al., 2009; Sachidhanandam et al., 2013). The difference may be due to our behavioral task, which demands that the whisker system operate in the receptive mode, actively keeping whiskers stationary. The increased excitation in the high state was also accompanied by an increased inhibition. Fast spiking parvalbumin-expressing interneurons receive strong direct sensory input from the thalamus and are responsible for feedforward inhibition (Sermet et al., 2019; Yu et al., 2019). The increased inhibition in the high state could be attributed to enhanced activation of these fast spiking interneurons. The observed spectrum of excitation and inhibition likely depends on the complex interaction between the excitatory and inhibitory inputs that a particular cell receives (Muir et al., 2013; Zagha et al., 2016). We speculate that the simultaneous and opposite rescaling of the response magnitude of excited and inhibited neurons reflects a mechanism that conserves homeostatic balance across the range of states that the sensory cortex naturally cycles through (Xue et al., 2014; Zhou et al., 2014).

The relationship between state and sensory representations is not fully understood. Some studies report an increased sensory response in desynchronized states due to lower noise correlations (Beaman et al., 2017; Engel et al., 2016), while others report the opposite (Hentschke et al., 2006; Sachidhanandam et al., 2013). In our study, evoked responses increased in a non-linear fashion, improving detection sensitivity as animals transitioned from low to high states (Figures 2H and 2I). As the state transitioned from low to high, the neuronal population showed less synchrony (Figures 3A and 3B). Spontaneous fluctuations in firing rate and intracellular potential are known to reflect the cortical state (DeWeese and Zador, 2006; Luczak et al., 2009; Poulet and Petersen, 2008). These pockets of population activity in the synchronized state, interspersed with periods of silence, impose a high level of correlated activity between adjacent neurons (Schölvinck et al., 2015). We found that the degree of synchrony decreased with distance (Figure 3C), which is consistent with the idea that nearby neurons share similar excitatory and inhibitory inputs. Overall, our findings are consistent with the distance-dependent decline seen in other studies (Rothschild et al., 2010; Sabri et al., 2016). However, these studies examine larger-scale spatial-temporal correlations that may be driven by connectivity between adjacent barrels and barrel-septum connectivity (Sabri et al., 2016). Here, we document state-dependent dynamics on the scale of a single barrel column (~250 μm).

We performed classification analysis as a function of stimulus intensity, the size of the coding population, and behavioral state (Figures 3E and 3G). In high states, there was a lower degree of correlated activity among neurons, and decoding performance sharply increased and plateaued at a higher level of accuracy compared to the low state. This is consistent with previous studies in which the desynchronized state reduced correlated fluctuations in neural activity, thereby allowing more accurate decoding (Mitchell et al., 2009). In our study, the removal of correlated activity by trial shuffling led to a greater increase in decoding performance in low states (Figure 3F), indicating that the diminished transmission of information in low states originated both from lower average stimulus-evoked signals (Figure 2) and from high noise correlation. The observed sharp increase in decoding may reflect the tendency of calcium imaging toward more active and potentially more informative neurons. The sharp increase may also reflect neural heterogeneity, in which a small but highly informative subset of neurons carry most of the information contained in the population (Ince et al., 2013).

There is a complex interaction between cortical state, whisker movement, sensory evoked responses, and the correlation in across-population activity. Whisker movement affects the membrane potential of vS1 neurons and their evoked response to passive stimulation (Crochet and Petersen, 2006). Beyond single-cell responses, pairwise correlation among vS1 neurons is typically higher in quiet, immobile wakefulness compared to active exploration and whisking activity (Poulet and Petersen, 2008). While behavioral state is often determined by the absence and presence of whisker movement (Poulet and Crochet, 2019), a further distinction can be made within periods of no whisker movement to separate epochs of active engagement in detection from periods of passive resting. In our task, when animals are highly engaged (high state), whisker movements may be actively suppressed to optimize stimulus detection (Kyriakatos et al., 2017).

Finally, we found that state modulated both vS1 activity and behavioral choices. Consistent with recent research, vS1 neurons showed robust choice-related activity (Poulet and Crochet, 2019; Yamashita and Petersen, 2016; Yang et al., 2016); higher responses were associated with hits and lower responses were associated with misses (Figures 4A–4C). The observed choice-related activity was further modulated by behavioral state, and this was observed consistently across all stimulus intensities (Figures 4C and 4D). The extent to which various sensory decision tasks require the direct involvement of the sensory cortex remains debatable. While some studies show dependence on vS1 for behaviors such as gap crossing (Hutson and Masterton, 1986), object localization (O'Connor et al., 2010), and vibration discrimination (Miyashita and Feldman, 2013), other studies identify cases in which vS1 is not required for the active detection of objects and passive detection of air puff

stimuli (Hong et al., 2018; Hutson and Masterton, 1986). This disparity likely rests on specific differences in the experimental context such as goal-directed versus habitual reflexive behaviors (Yeomans et al., 2002), appetitive versus aversive conditioning (Guic-Robles et al., 1992; Hutson and Masterton, 1986), or stimulus duration and reward schedules (Krupa et al., 2001; Miyashita and Feldman, 2013). The capacity of the brain to generate alternative processing pathways or strategies in response to the loss of function of vS1 must also be considered. Nevertheless, if vS1 is not required for sensory decision making, then one alternative explanation for the observed results is that neuronal activity in the somatosensory cortex and behavioral outcomes may both be modulated by state independently. State may affect behavioral outcomes via subcortical processing circuits such as brainstem (Tsunematsu et al., 2020), thalamic nuclei (Sieveritz et al., 2019), and superior colliculus (Wang et al., 2020). The state modulations in subcortical circuits may then be transmitted to the sensory cortex, producing choice-related activity in vS1 (Yang et al., 2016). In this respect, long-range synchronization between brain regions may underlie the functional coupling of areas co-engaged in a given task (Melloni et al., 2007). For example, motor cortex feedback influences sensory processing by modulating network state, and the coherence between rat sensorimotor system and hippocampus is enhanced during tactile discrimination (Grion et al., 2016). Future experiments can investigate how long-range synchronization and decision outcomes are affected by specific demands of the paradigm and the animal's engagement in the task.

A key circuit motif for state modulation is through disinhibition (Jackson et al., 2016; Muir et al., 2013). The vasoactive intestinal peptide (VIP) expressing inhibitory neurons in super-granular layers of the sensory cortex receive corticocortical inputs from motor areas (Lee et al., 2013) or cholinergic projections from basal forebrain (Zagha and McCormick, 2014). The activation of VIP interneurons inhibits the somatostatin (SOM)-expressing neurons located in L2/3. Consequently, this disinhibits the inhibition that L2/3 pyramids receive from SOM interneurons and thus transitions the network into a more active desynchronized state. Alternatively, a range of neuromodulatory inputs that arrive in the sensory cortex can influence the cortical state (Lee and Dan, 2012). For example, noradrenergic afferents originating from the locus coeruleus contribute to state transition and have been shown to increase neuronal excitability in the somatosensory cortex (Fazlali et al., 2016) and improve sensory detection and processing (Safaai et al., 2015). Future work can identify the role of specific subtypes of inhibitory neurons across layers of vS1 in the detection task to reveal the neural circuits of sensorimotor transformation from whisker stimulus to goal-directed licking.

STAR★METHODS

Detailed methods are provided in the online version of this paper and include the following:

- KEY RESOURCES TABLE
- RESOURCE AVAILABILITY
  - Lead Contact
  - Materials Availability
  - Data and Code Availability
- EXPERIMENTAL MODEL AND SUBJECT DETAILS
  - Mice
- METHOD DETAILS
  - Surgery
  - Apparatus
  - Training and behavioral task
  - Whisker Tracking
  - Pupillography
- QUANTIFICATION AND STATISTICAL ANALYSIS
  - Behavioral analysis
  - Neuronal response analysis
  - Cross-correlation analysis
  - Noise-correlation and classification analysis

SUPPLEMENTAL INFORMATION

Supplemental Information can be found online at https://doi.org/10.1016/j.celrep.2020.108197.

ACKNOWLEDGMENTS

The experiments were supported by an Australian Research Council (ARC) Discovery Project (DP170100908), NHMRC project grants (APP1124411), an NHMRC ideas grant (APP1181643), the ARC Centre of Excellence for Integrative Brain Function (ARC Centre Grant, CE140100007), the European Research Council advanced grant CONCEPT (Project 294498), and the Human Frontier Science Program (Project RGP0015/2013).

AUTHOR CONTRIBUTIONS

C.C.Y.L. and E.A. conceived and designed the project. C.C.Y.L. and E.K. performed the experiments. C.C.Y.L., M.E.D., and E.A. analyzed the data. C.C.Y.L., M.E.D., and E.A. wrote the manuscript. All of the authors edited the manuscript and approved the final version.

DECLARATION OF INTERESTS

The authors declare no competing interests.

Received: February 14, 2020
Revised: July 7, 2020
Accepted: September 3, 2020
Published: September 29, 2020

REFERENCES

Adibi, M., Diamond, M.E., and Arabzadeh, E. (2012). Behavioral study of whisker-mediated vibration sensation in rats. Proc. Natl. Acad. Sci. USA *109*, 971–976.

Averbeck, B.B., Latham, P.E., and Pouget, A. (2006). Neural correlations, population coding and computation. Nat. Rev. Neurosci. *7*, 358–366.

Beaman, C.B., Eagleman, S.L., and Dragoi, V. (2017). Sensory coding accuracy and perceptual performance are improved during the desynchronized cortical state. Nat. Commun. *8*, 1308.

Carvell, G.E., and Simons, D.J. (2017). Effect of whisker geometry on contact force produced by vibrissae moving at different velocities. J. Neurophysiol. *118*, 1637–1649.

Clack, N.G., O'Connor, D.H., Huber, D., Petreanu, L., Hires, A., Peron, S., Svoboda, K., and Myers, E.W. (2012). Automated tracking of whiskers in videos of head fixed rodents. PLOS Comput. Biol. *8*, e1002591.

Crochet, S., and Petersen, C.C.H. (2006). Correlating whisker behavior with membrane potential in barrel cortex of awake mice. Nat. Neurosci. *9*, 608–610.

DeWeese, M.R., and Zador, A.M. (2006). Non-Gaussian membrane potential dynamics imply sparse, synchronous activity in auditory cortex. J. Neurosci. *26*, 12206–12218.

Diamond, M.E., and Arabzadeh, E. (2013). Whisker sensory system - from receptor to decision. Prog. Neurobiol. *103*, 28–40.

Diamond, M.E., von Heimendahl, M., and Arabzadeh, E. (2008). Whisker-mediated texture discrimination. PLOS Biol. *6*, e220.

Eggermann, E., Kremer, Y., Crochet, S., and Petersen, C.C.H. (2014). Cholinergic signals in mouse barrel cortex during active whisker sensing. Cell Rep. *9*, 1654–1660.

Engel, T.A., Steinmetz, N.A., Gieselmann, M.A., Thiele, A., Moore, T., and Boahen, K. (2016). Selective modulation of cortical state during spatial attention. Science *354*, 1140–1144.

Fassihi, A., Akrami, A., Esmaeili, V., and Diamond, M.E. (2014). Tactile perception and working memory in rats and humans. Proc. Natl. Acad. Sci. USA *111*, 2331–2336.

Fazlali, Z., Ranjbar-Slamloo, Y., Adibi, M., and Arabzadeh, E. (2016). Correlation between cortical state and locus coeruleus activity: Implications for sensory coding in rat barrel cortex. Front. Neural Circuits *10*, 14.

Grion, N., Akrami, A., Zuo, Y., Stella, F., and Diamond, M.E. (2016). Coherence between Rat Sensorimotor System and Hippocampus Is Enhanced during Tactile Discrimination. PLoS Biol. *14*, e1002384.

Guic-Robles, E., Jenkins, W.M., and Bravo, H. (1992). Vibrissal roughness discrimination is barrelcortex-dependent. Behav. Brain Res. *48*, 145–152.

Harris, K.D., and Thiele, A. (2011). Cortical state and attention. Nat. Rev. Neurosci. *12*, 509–523.

Hentschke, H., Haiss, F., and Schwarz, C. (2006). Central signals rapidly switch tactile processing in rat barrel cortex during whisker movements. Cereb. Cortex *16*, 1142–1156.

Hong, Y.K., Lacefield, C.O., Rodgers, C.C., and Bruno, R.M. (2018). Sensation, movement and learning in the absence of barrel cortex. Nature *561*, 542–546.

Hutson, K.A., and Masterton, R.B. (1986). The sensory contribution of a single vibrissa's cortical barrel. J. Neurophysiol. *56*, 1196–1223.

Ince, R.A.A., Panzeri, S., and Kayser, C. (2013). Neural codes formed by small and temporally precise populations in auditory cortex. J. Neurosci. *33*, 18277–18287.

Jackson, J., Ayzenshtat, I., Karnani, M.M., and Yuste, R. (2016). VIP+ interneurons control neocortical activity across brain states. J. Neurophysiol. *115*, 3008–3017.

Kayser, C., Petkov, C.I., Lippert, M., and Logothetis, N.K. (2005). Mechanisms for allocating auditory attention: an auditory saliency map. Curr. Biol. *15*, 1943–1947.

Kohn, A., Coen-Cagli, R., Kanitscheider, I., and Pouget, A. (2016). Correlations and Neuronal Population Information. Annu. Rev. Neurosci. *39*, 237–256.

Krupa, D.J., Matell, M.S., Brisben, A.J., Oliveira, L.M., and Nicolelis, M.A.L. (2001). Behavioral properties of the trigeminal somatosensory system in rats performing whisker-dependent tactile discriminations. J. Neurosci. *21*, 5752–5763.

Kwon, S.E., Yang, H., Minamisawa, G., and O'Connor, D.H. (2016). Sensory and decision-related activity propagate in a cortical feedback loop during touch perception. Nat. Neurosci. *19*, 1243–1249.

Kyriakatos, A., Sadashivaiah, V., Zhang, Y., Motta, A., Auffret, M., and Petersen, C.C.H. (2017). Voltage-sensitive dye imaging of mouse neocortex during a whisker detection task. Neurophotonics *4*, 031204.

Lee, S.H., and Dan, Y. (2012). Neuromodulation of brain states. Neuron *76*, 209–222.

Lee, S., Kruglikov, I., Huang, Z.J., Fishell, G., and Rudy, B. (2013). A disinhibitory circuit mediates motor integration in the somatosensory cortex. Nat. Neurosci. *16*, 1662–1670.

Lee, C.C.Y., Diamond, M.E., and Arabzadeh, E. (2016). Sensory Prioritization in Rats: Behavioral Performance and Neuronal Correlates. J. Neurosci. *36*, 3243–3253.

Lee, C.C.Y., Clifford, C.W.G., and Arabzadeh, E. (2019). Temporal cueing enhances neuronal and behavioral discrimination performance in rat whisker system. J. Neurophysiol. *121*, 1048–1058.

Luczak, A., Barthó, P., and Harris, K.D. (2009). Spontaneous events outline the realm of possible sensory responses in neocortical populations. Neuron *62*, 413–425.

McGinley, M.J., Vinck, M., Reimer, J., Batista-Brito, R., Zagha, E., Cadwell, C.R., Tolias, A.S., Cardin, J.A., and McCormick, D.A. (2015). Waking State: Rapid Variations Modulate Neural and Behavioral Responses. Neuron *87*, 1143–1161.

Melloni, L., Molina, C., Pena, M., Torres, D., Singer, W., and Rodriguez, E. (2007). Synchronization of neural activity across cortical areas correlates with conscious perception. J. Neurosci. *27*, 2858–2865.

Mitchell, J.F., Sundberg, K.A., and Reynolds, J.H. (2009). Spatial attention decorrelates intrinsic activity fluctuations in macaque area V4. Neuron *63*, 879–888.

Miyashita, T., and Feldman, D.E. (2013). Behavioral detection of passive whisker stimuli requires somatosensory cortex. Cereb. Cortex *23*, 1655–1662.

Muir, J.L., Lee, C.C.Y.Y., Diamond, M.E., Arabzadeh, E., Rodgers, C.C., DeWeese, M.R.R., McDonald, J.S., Adibi, M., Clifford, C.W.G.G., Arabzadeh, E., et al. (2013). Whisker Movements Reveal Spatial Attention: A Unified Computational Model of Active Sensing Control in the Rat. J. Neurosci. *9*, 38.

Muñoz, W., Tremblay, R., Levenstein, D., and Rudy, B. (2017). Layer-specific modulation of neocortical dendritic inhibition during active wakefulness. Science *355*, 954–959.

O'Connor, D.H., Clack, N.G., Huber, D., Komiyama, T., Myers, E.W., and Svoboda, K. (2010). Vibrissa-based object localization in head-fixed mice. J. Neurosci. *30*, 1947–1967.

Otazu, G.H., Tai, L.H., Yang, Y., and Zador, A.M. (2009). Engaging in an auditory task suppresses responses in auditory cortex. Nat. Neurosci. *12*, 646–654.

Pola, G., Thiele, A., Hoffmann, K.P., and Panzeri, S. (2003). An exact method to quantify the information transmitted by different mechanisms of correlational coding. Network Comput. Neural Syst. *14*, 35–60.

Poulet, J.F.A., and Crochet, S. (2019). The cortical states of wakefulness. Front. Syst. Neurosci. *12*, 64.

Poulet, J.F.A., and Petersen, C.C.H. (2008). Internal brain state regulates membrane potential synchrony in barrel cortex of behaving mice. Nature *454*, 881–885.

Poulet, J.F.A., Fernandez, L.M.J., Crochet, S., and Petersen, C.C.H. (2012). Thalamic control of cortical states. Nat. Neurosci. *15*, 370–372.

Randall, J.A. (2010). Drummers and stompers: vibrational communication in mammals. In The Use of Vibrations in Communication: Properties, Mechanisms and Function across Taxa, C.E. O'Connell-Rodwell, ed. (Transworld Research Network), pp. 99–120.

Rothschild, G., Nelken, I., and Mizrahi, A. (2010). Functional organization and population dynamics in the mouse primary auditory cortex. Nat. Neurosci. *13*, 353–360.

Sabri, M.M., and Arabzadeh, E. (2018). Information processing across behavioral states: modes of operation and population dynamics in rodent sensory cortex. Neuroscience *368*, 214–228.

Sabri, M.M., Adibi, M., and Arabzadeh, E. (2016). Dynamics of population activity in rat sensory cortex: network correlations predict anatomical arrangement and information content. Front. Neural Circuits *10*, 49.

Sachidhanandam, S., Sreenivasan, V., Kyriakatos, A., Kremer, Y., and Petersen, C.C.H. (2013). Membrane potential correlates of sensory perception in mouse barrel cortex. Nat. Neurosci. *16*, 1671–1677.

Safaai, H., von Heimendahl, M., Sorando, J.M., Diamond, M.E., and Maravall, M. (2013). Coordinated population activity underlying texture discrimination in rat barrel cortex. J. Neurosci. *33*, 5843–5855.

Safaai, H., Neves, R., Eschenko, O., Logothetis, N.K., and Panzeri, S. (2015). Modeling the effect of locus coeruleus firing on cortical state dynamics and single-trial sensory processing. Proc. Natl. Acad. Sci. USA *112*, 12834–12839.

Schölvinck, M.L., Saleem, A.B., Benucci, A., Harris, K.D., and Carandini, M. (2015). Cortical state determines global variability and correlations in visual cortex. J. Neurosci. *35*, 170–178.

Sermet, B.S., Truschow, P., Feyerabend, M., Mayrhofer, J.M., Oram, T.B., Yizhar, O., Staiger, J.F., and Petersen, C.C.H. (2019). Pathway-, layer- and cell-type-specific thalamic input to mouse barrel cortex. eLife *8*, e52665.

Sieveritz, B., García-Muñoz, M., and Arbuthnott, G.W. (2019). Thalamic afferents to prefrontal cortices from ventral motor nuclei in decision-making. Eur. J. Neurosci. *49*, 646–657.

Speed, A., Del Rosario, J., Burgess, C.P., and Haider, B. (2019). Cortical State Fluctuations across Layers of V1 during Visual Spatial Perception. Cell Rep. *26*, 2868–2874.e3.

Stringer, C., and Pachitariu, M. (2019). Computational processing of neural recordings from calcium imaging data. Curr. Opin. Neurobiol. *55*, 22–31.

Tsunematsu, T., Patel, A.A., Onken, A., and Sakata, S. (2020). State-dependent brainstem ensemble dynamics and their interactions with hippocampus across sleep states. eLife *9*, e52244.

von Heimendahl, M., Itskov, P.M., Arabzadeh, E., and Diamond, M.E. (2007). Neuronal activity in rat barrel cortex underlying texture discrimination. PLOS Biol. *5*, e305.

Wang, L., McAlonan, K., Goldstein, S., Gerfen, C.R., and Krauzlis, R.J. (2020). A causal role for mouse superior colliculus in visual perceptual decision-making. J. Neurosci. *40*, 3768–3782.

Xue, M., Atallah, B.V., and Scanziani, M. (2014). Equalizing excitation-inhibition ratios across visual cortical neurons. Nature *511*, 596–600.

Yamashita, T., and Petersen, C.Ch. (2016). Target-specific membrane potential dynamics of neocortical projection neurons during goal-directed behavior. eLife *5*, e15798.

Yang, H., Kwon, S.E., Severson, K.S., and O'Connor, D.H. (2016). Origins of choice-related activity in mouse somatosensory cortex. Nat. Neurosci. *19*, 127–134.

Yeomans, J.S., Li, L., Scott, B.W., and Frankland, P.W. (2002). Tactile, acoustic and vestibular systems sum to elicit the startle reflex. Neurosci. Biobehav. Rev. *26*, 1–11.

Yu, J., Hu, H., Agmon, A., and Svoboda, K. (2019). Recruitment of GABAergic Interneurons in the Barrel Cortex during Active Tactile Behavior. Neuron *104*, 412–427.e4.

Zagha, E., and McCormick, D.A. (2014). Neural control of brain state. Curr. Opin. Neurobiol. *29*, 178–186.

Zagha, E., Murray, J.D., and McCormick, D.A. (2016). Simulating cortical feedback modulation as changes in excitation and inhibition in a cortical circuit model. ENeuro *3*, 0208–0216.

Zhou, M., Liang, F., Xiong, X.R., Li, L., Li, H., Xiao, Z., Tao, H.W., and Zhang, L.I. (2014). Scaling down of balanced excitation and inhibition by active behavioral states in auditory cortex. Nat. Neurosci. *17*, 841–850.

Zuo, Y., Safaai, H., Notaro, G., Mazzoni, A., Panzeri, S., and Diamond, M.E. (2015). Complementary contributions of spike timing and spike rate to perceptual decisions in rat S1 and S2 cortex. Curr. Biol. *25*, 357–363.

CellPress
OPEN ACCESS

STAR★METHODS

KEY RESOURCES TABLE

REAGENT or RESOURCE	SOURCE	IDENTIFIER
Bacterial and Virus Strains		
GCaMP6f (AAV1.Syn.GCaMP6f.WPRE.SV40)	Penn Vector Core, The University of Pennsylvania, USA	Addgene; CAT# 100837-AAV1
Biological Samples		
Mouse: C57BL/6J	The Jackson Laboratory	Stock No: 000664
Chemicals, Peptides, and Recombinant Proteins		
Isoflurane	Henry Schein, Australia	REF: 998-3244
Software and Algorithms		
MATLAB v2019a	MathWorks, Inc., Natick, MA	https://www.mathworks.com/products/matlab.html
Deposited Data		
Behavioural and calcium data		https://doi.org/10.17605/OSF.IO/DE5RH

RESOURCE AVAILABILITY

Lead Contact

Further information and requests for resources and reagents should be directed to and will be fulfilled by the Lead Contact, Conrad Chun Yin Lee (conrad.lee@anu.edu.au).

Materials Availability

This study did not generate new unique reagents.

Data and Code Availability

The dataset generated during this study is available at: https://osf.io/de5rh.The accession number for the behavioural and calcium data reported in this paper is available at OSF: [DOI 10.17605/OSF.IO/DE5RH].

The MATLAB codes generated during this study are available from lead contact on request.

EXPERIMENTAL MODEL AND SUBJECT DETAILS

Mice

Subjects were seven 4 week old male C57BL6J with initial weights of 20-25 g. All procedures were approved by the Animal Care and Ethics Committee at the Australian National University. Mice were house in independently ventilated and air filtered transparent plastic boxes in a climate controlled colony room on a 12/12 hour light/dark cycle, where lights were turned off at 7pm. Mice were water restricted to motivate animal to perform the detection task. Mice had abundant access to water for 2-3hrs after training sessions and were provided with ad-lib food. All mice gained weight at a normal rate throughout the entire duration of the experiment.

METHOD DETAILS

Surgery

Mice underwent surgery for viral infection and head-post implantation. They were anesthetized with isoflurane (~2% by volume in O_2) and their eyes were covered with a thin layer of Viscotears liquid gel (Alcon, UK) and kept on a thermal blanket to maintain body temperature (Physitemp Instruments). The scalp and periosteum over the dorsal surface of the skull were removed. A circular craniotomy was made over the right barrel cortex (3mm diameter; center relative to Bregma: lateral 3mm; posterior 1.8mm) with the dura left intact. GCamp6*f* (AAV1.Syn.GCamp6f.WPRE.SV40) were injected in 4-6 sites within the craniotomy (4 injections at 32nL per site; depth, 230-250μm; rate ~92 nLs^{-1}) using a glass pipette (15-25μm, tip diameter) via a Nanoject II injector (Drumont scientific, PA). After viral injection, the craniotomy was covered with a glass imaging window 3mm in diameter and 150 ± 20μm in thickness (Warner Instruments, CT). This was glued to the bone surrounding the craniotomy. Custom made head posts were fixed to the skull above lambda using a thin layer of cyanoacrylate adhesive and secured to the skull using dental acrylic. A small well was built surrounding the craniotomy window using dental acrylic to accommodate distilled water required for immersion lens for two-photon microscope imaging.

Apparatus

Mice were trained to perform a vibration detection task while head-fixed. All behavioral apparatus was controlled by custom written script in MATLAB (The Mathworks) and interfaced through a data acquisition card (National Instruments, Austin, TX) at a sampling rate of 100kHz. The vibration stimulus was presented to the left whisker pad via an aluminum mesh (2x2cm) attached to a ceramic piezoelectric wafer (Morgan Matroc, Bedford, OH). The mesh was slanted parallel to the animal's left whisker pad (~2mm from the surface of the snout). Spacing on the mesh was arranged in a grid with each opening adjacent to one another. Each opening was approximately 150μm apart. At 2mm from the surface of the snout, the diameter of the whiskers of a mouse is approximately 80μm (Carvell and Simons, 2017). Using a microscope, we adjusted the position of the vibrating mesh to reliably engage the maximums number of whiskers to reduce the possibility of poor whisker engagement. Any whiskers that did not enter through an opening on the mesh were rested against the wire structure of the mesh. The vibration stimulus was a series of discrete Gaussian deflections. Each deflection lasted for 15ms and was followed by a 10ms pause before the next deflection, yielding a frequency of 40Hz. The total stimulus duration was 300ms. The stimulus amplitude ranged from 0μm, 10μm, 20μm, 40μm, and 80 μm. A custom steel "lick-port" was used to record licks and to deliver 5% sucrose reward and was attached to a micromanipulator to adjust distance for each animal. The lick-port was placed within reach of the tongue at ~0.5mm below the lower lip and ~5mm posterior to the tip of the nose. The lick-port was connected to an Arduino Uno acting as a capacitive sensor. The capacitive voltage was sent to data acquisition card and a software threshold was set to determine if a lick was present or absent. The sucrose was delivered via a gravity feed solenoid valve. Mice were placed in an acrylic (4cm inner diameter) tubes such that their heads extended out the front and they could use their front paws to grip the tube edge. A surgically implanted custom head post that extended to the sides of the mice was used to immobilize the animal. Mice were thereby head-fixed in a natural crouching position with their whiskers free to move around the space surround their head.

For recording, the animal was transferred to a two-photon imaging microscope system (ThorLabs, MA) with a Cameleon (Coherent) TiLSapphire laser tuned at 920nm and focused by a water-immersion Nikon objective (x16, 0.58NA). All image acquisition was performed via ThorImage (ThorLabs, MA) and frames were synchronized with the stimulus presentation via the data acquisition card.

Training and behavioral task

Training began after surgery and recovery. Animals experienced 4 days of water restriction. During this period, mice were handled to adapt to the experimenter and to the head fixation setup. This involved picking up mice and running the animal through the acrylic tube. With a hemostatic forcep, mice were held in position in the head-fixation post for increasingly longer duration (from 1seconds to 60seconds). Once mice adapted to hand held head-fixation, they were head-fixed into the post for increasingly longer duration (from 1minute to 10 minutes). At each fixation, mice were rewarded with 5% sucrose from a pipette held by the experimenter.

Training began once the animal adapted to head-fixation with one session during which the mouse was rewarded for every lick recorded on the lick-port. When the animal licked, the vibration stimulus was presented for 1 s. By the end of the sessions, mice reliably triggered and consumed the sucrose reward. At the next phase of training, the vibration stimulus was presented indefinitely, until the mice licked the lick-port to trigger release of sucrose. The mice had to trigger the reward three times, after which a 60 s no-go period was enforced. During this period, no stimulus was presented and any licks of the lick-port did not release any sucrose. This reinforced the association that licking during the vibration stimulus resulted in a reward, while licking when the stimulus was absent resulted in no reward. In three to four sessions, mice reliably triggered reward during the stimulus period and refrained when no stimulus was present. Next, the stimulus period was reduced to 1 s, and the stimulus was either 80μm (go) or 0um (no-go). Between each stimulus presentation, a variable inter-trial interval was enforced, which varied between 5-7 s. After mastering this easy version of the task (above ~85% correct), the stimulus period was reduced from 1 s to 300ms over four sessions and the inter-trial-interval was increased to 5-10 s. Once mastered, mice advanced to the final version of the task in which 5 stimulus amplitudes (0μm, 10μm, 20μm, 40μm, 80μm) were introduced. Amplitudes were pseudo randomized in 5 trials blocks, such that each block contained all possible stimulus amplitude. Mice performed the detection task for an extended period each day (~400 trials), in order to obtain different periods of global arousal states. This was critical as mice experienced the same stimulus intensities and have the same opportunity to response across the entire session.

Whisker Tracking

A high speed camera (Mikrotron EoSens CL, Unterschleissheim Germany) was placed above the whisker pad capturing 1000 frames per second at a resolution of 400x480 pixels. A panel of infra-red LEDs illuminated the floor below the whisker pad. 1 s videos clips were captured centered at each stimulus onset. We quantified whisker movement by first filtering each frame via edge detection and measuring the percentage change in pixel intensity from one frame to another in a 200x50 pixel ROI that contained only the ipsilateral whisker pad (Figure S3A; Video S2). Whisker movement was quantified from a 300ms window before the stimulus onset. All whisker tracking and behavior was performed in darkness. In total, we captured whisking data for 3 mice over 12 sessions each. On average each session was ~90mins long, totaling 54hrs of high-speed video data. Pixel change analysis captures both whisking amplitude and velocity. We cannot separate these two factors from our measurement. However, from our observation in Video S2, pixel change analysis in Figure S5 and tracking via WHISK (Clack et al., 2012), we observed no whisking activity nor differences in pixel change/whisker movement.

CellPress
OPEN ACCESS

Pupillography

A camera (DMK22BUC03, The Image Source, Taiwan) capturing at 30 frames per second, was place at an oblique angle focusing on the mouse's left eye. The infra-red light used to illuminate the floor for whisker tracking was also used to illuminate the pupil. All pupil tracking and behavior was performed in darkness. We took precaution in turning off computer monitors and another other light source that could influence pupil dilation. Pupil area was isolated using a custom written MATLAB code that utilized a combination of frame scaling and circle Hough transformation.

QUANTIFICATION AND STATISTICAL ANALYSIS

Behavioral analysis

Hit trials were defined as the presence of at least one lick 0-300ms post stimulus onset and no licks 300ms before stimulus onset. Miss trials were defined as the absence of lick 0-300ms post stimulus onset. Behavioral stimulus detectability was computed from distributions of lick counts occurring 1 s before and after each stimulus onset. A criterion shifted in steps of one lick across the two distributions was used to determine the hit and false alarms of a stimulus condition, thus forming a receiver operating characteristic (ROC) curve. Detectability was expressed as the area under the ROC. State was classified into three categories based on the mice performance by calculating the detection rate within each block (0%: no detection; 100%: all four amplitudes detected): low-state (0%–25%), intermediate-state (50%) and high-state (75%–100%). Since the 5 stimulus intensities were randomized in blocks of 5 trials, state performance was calculated as the average detection performance for each 5 trial block. The ranges of state performance were then separated into the three categories – 0%–25%, 50%, 75%–100%.

On selected sessions, we observed a general decline in motivation over time. This was characterized by changes in false alarm (behavioral response to zero stimulus intensity) over time. To account for changes in motivation and task engagement, we restricted our analysis to trials in which false alarm was zero. For majority of trials, this was the case – mice correctly rejected zero stimulus intensity by withholding licking. In each 5 trial block (containing all stimulus intensities: 0, 10, 20, 40, 80μm), we excluded blocks of trials in which the mice responded to the 0um stimulus (false alarm). Calcium response profile for each behavioral state was then calculated with the remaining blocks of trials (Figure S4F).

As state was defined by stimulus present trials including the trial of interest, the observed effect of outcome modulation may be confounded by the current trial of interest. To mitigate this, we performed an additional analysis to supplement our choice outcome analysis (Figure S4B). This analysis was performed at each 5 trial block to contain all stimulus intensity: 0, 10, 20, 40, 80μm. Like before, for every trial within each block, we defined behavioral state by calculating the detection performance for all stimulus present trials (10, 20 40 80μm). However, in this complementary analysis, the current trial was excluded in the calculation. This resulted in 4 behavioral state categories: 0%, 33.3%, 66.6%, and 100%.

Neuronal response analysis

Image stacks were corrected for motion and regions of interest (ROIs) were selected for each cell in each session using Suite2P (Stringer and Pachitariu, 2019). Raw fluorescence F was obtained for each cell by averaging across pixels within each ROI. Baseline fluorescence F_0 was calculated by determining the average F in the preceding 500ms time window from stimulus onset. The change in fluorescence relative to baseline, $\Delta F/F$, was computed by taking the difference between F and F_0 and dividing by F_0. For all fluorescence heatmaps and average traces, plots were generated by a sliding window average of 10 frames at steps of 1 frame.

Cross-correlation analysis

Cross correlation between pupil diameter and performance was calculated from a 5 trial sliding window. Pupil diameter was calculated as the average diameter in each window. To perform cross correlation, both measurements were normalized to vary between 0-1. Correlations were also bias corrected for different lag lengths. To calculate correlation coefficient between neuron pairs, we computed the normalized cross correlogram of each cell pairs during periods of spontaneous activity (0-4 s window before stimulus onset). Baseline fluorescence F_0 was calculated by determining the average F in the preceding 4-5 s time window from stimulus onset. Finally, we calculated the maximum height of the correlogram as a measure of correlation strength.

Noise-correlation and classification analysis

For noise correlation, in order to remove any effect of stimulus on correlation, we only performed the pairwise correlations on the spontaneous activity (4 s before stimulus onset). For each cell pair, the mean fluorescence activity is calculated on each trial and correlated. Classification analysis employed a linear discrimination classifier, training with 90% of data points and testing on the remaining 10%. The classifier classified calcium response from a 1 s window post stimulus onset. This response was baseline corrected (1 s pre stimulus onset). We classified stimulus present trials (10-80μm) against stimulus absent trials (0μm). The decoding accuracy for each neuron population size was calculated as the average performance over 100 classifying iterations. Figure 3D shows an example session of decoding 20μm stimulus present trials against 0μm stimulus absent trials. Figure 3E shows the average across all sessions for decoding 20μm stimulus present trials against 0μm stimulus absent trials. To examine the contribution of noise-correlation to decoding accuracy, we decorrelated the activity of neurons by shuffling the trial order within each trial category (ie. shuffling within stimulus present trials and stimulus absent trials for each stimulus amplitude and behavioral state). Trial order was

averaged over 100 shuffles for neuron population size iteration. Figure 3F shows the improvement of decoding accuracy for 20μm versus 0μm stimulus across all imaging session and population size. Decorrelating the activity by shuffling trial order improved decoding accuracy in low- state compared to high-state.

Relevant statistical analyses, *p* values, and n sizes are reported in figure legends and results section. Data were analyzed and presented as mean ± standard deviation (SD) or standard error of the mean (SEM) in all figures. Statistical significance was determined using MATLAB software. Results with a p value lower than 0.05 were considered significant.